# In Vivo Biorthogonal Antibody Click for Dual Targeting and Augmented Efficacy in Cancer Treatment

Sandeep Surendra Panikar[1], Na-Keysha Berry[1], Shayla Shmuel[1], Nai Keltee[1], Patrícia M.R. Pereira[1,*]

**Affiliations:**

[1]Department of Radiology, Mallinckrodt Institute of Radiology, Washington University School of Medicine, St. Louis, MO 63110, USA

***Corresponding Author:**

Patrícia M. R. Pereira; ribeiropereirap@wustl.edu; P: +1 314-273-4898

**Disclosures:** None.

**Conflict of interest:** The authors declare no potential conflicts of interest.

**Financial Support:**

This research was supported by internal funds provided by the Mallinckrodt Institute of Radiology, NIH (R37CA276498), and by the Breast Cancer Alliance. PMRP acknowledges NIH (R37CA276498) and the Breast Cancer Alliance. The Preclinical Imaging Facility was supported by NIH/NCI Siteman Cancer Center (SCC) Support Grant P30CA091842, NIH instrumentation grants S10OD018515 and S10OD030403, and internal funds provided by Mallinckrodt Institute of Radiology.

**Acknowledgments:**

We thank the Washington University School of Medicine isotope production team for the production of zirconium-89 and copper-64, the small animal imaging facility for help with the small animal PET/CT image collection, and the Washington University Center for Cellular Imaging (WUCCI) for their assistance with the TEM images. We thank Dr. Luis Batista for letting us use the Odyssey Infrared Imaging System. We thank Dr. Luke Carter for his help with the 3D Slicer software. We thank Dr. Ricardo D'Oliveira Albanus for their help with data presentation and figure preparation. We gratefully acknowledge the Siteman Cancer Center pharmacy for providing us with trastuzumab/Herceptin and panitumumab/Vectibix antibodies.

**ABSTRACT**

Antibody-drug conjugates (ADCs) have emerged as promising therapeutics for cancer treatment; however, their effectiveness has been limited by single antigen targeting, potentially leading to resistance mechanisms triggered by tumor compensatory pathways or reduced expression of the target protein. Here, we present antibody-ADC click, an approach that harnesses bioorthogonal click chemistry for *in vivo* dual targeting of ADCs, irrespective of the tumor's expression of the ADC-targeting antigen. We conjugated the bioorthogonal click moieties tetrazine (Tz) and trans-cyclooctene (TCO) to both antibodies and ADCs. Through *in vivo* clicking of antibody-TCO with antibody-Tz, we achieved sequential dual-receptor targeting in tumors. We show that the clicked antibody therapy outperformed conventional ADC monotherapy in preclinical models mimicking ADC-eligible, ADC-resistant, and ADC-ineligible tumors. Antibody-ADC click allows reversal of drug resistance through multi-antigen targeting and enhanced ADC accumulation within tumors. Antibody-ADC click enables *in vivo* multi-targeting without extensive bioengineering, sustains tumor treatment, and enhances antibody-mediated cytotoxicity.

## INTRODUCTION

Antibody-drug conjugates (ADCs) have transformed cancer care, with over 14 FDA-approved ADCs being effective in the treatment of patients with cancer[1]. The global ADC market is projected to reach over $15 billion USD by 2030[2] attributed to the exceptional specificity of ADCs that allows targeted delivery of potent cytotoxic drugs to cells expressing the target antigen[3-5]. However, ADCs rely on single antigen targeting, which can result in resistance if tumors activate compensatory pathways in response[1, 6, 7] or if the expression of the target protein is decreased[8, 9].

To overcome limitations of single-antigen targeting by ADCs, both antibody (mAbs) combination therapies[10-12] and bispecific antibodies[13] have been explored and approved for cancer treatments. While mAbs plus ADC combinations targeting distinct epitopes or antigens have demonstrated higher efficacy when compared with ADC therapy alone[14, 15], the two therapeutic agents might not reach the same cancer cell nor are they in close proximity to maximize endocytosis of the therapeutic ADC payload[1, 6, 16]. In the context of bispecific antibodies, one bispecific[17] has attained regulatory approval to date for the treatment of solid tumors, with suboptimal pharmacokinetics, distribution, and significantly higher costs limiting translation compared to conventional ADC therapies[13]. Additionally, there are no clinically approved bispecific antibodies that are successfully conjugated with cytotoxic drugs in a manner similar to ADCs.

To overcome the challenges associated with single-antigen targeting and the complexities of bispecific antibodies, we developed an "antibody-ADC click" strategy leveraging the power *of in vivo* click chemistry to allow for sequential dual-targeting in tumors. This technology involves sequential administration of FDA-approved mAbs and ADC, followed by the *in vivo* click through

the precise biorthogonal click chemistry — recognized by the 2022 Nobel Prize[18-23] — in a living organism. Notably, bioorthogonal click chemistry creates unique opportunities to allow the development of therapies targeting distinct antigens using selective reactions *in vivo*[18, 19]. In this context, recent studies highlight clinical promise in utilizing tetrazine-transcyclooctene cycloaddition reaction for pre-targeted payload delivery [24].

Incorporating groundbreaking innovations in bioorthogonal chemistry, our study advances the use of combinatorial approaches of mAbs and ADC by integrating tetrazine and *trans*-cyclooctene click moieties. This approach allows for sequential multi-receptor targeting within tumors, surpassing the capabilities of conventional ADCs. Our findings establish *in vivo* biorthogonal clicking of mAbs and ADCs, targeting distinct epitopes or antigens, as a promising approach for treating tumors non-responsive to or resistant to conventional ADC therapies. "Antibody-ADC click" reported here lays the foundation for further integration into distinct antibody and/or ADC combinations offering multiple avenues for therapeutic exploration of cancer and other diseases.

**Optimization of Bioorthogonal Clicking of FDA-approved Antibodies**

ADCs currently approved by the FDA rely on targeting a single receptor at a time to deliver a cytotoxic payload to cancer cells[5]. Here, we optimized FDA-approved antibodies (mAbs) and ADCs with bioorthogonal clicking moieties to enable effective sequential *in vivo* dual-targeting of heterogeneous cancers expressing multiple receptors (**Fig. 1a**). Our approach offers several advantages when compared with conventional ADC monotherapies. First, antibody-ADC bioconjugation takes place within the living organism, enabling multi-targeting without the need for extensive bioengineering of the mAbs. Second, it allows for dual blockade of receptors enabling a more sustained tumor treatment compared to conventional ADC therapy. Third, the ADC targets not only cancer cells that express the target antigen, but it also clicks with the respective mAb pair on the cellular surface regardless of ADC-targeting receptor presence. Fourth, using an antibody click approach results in a large number of receptor-antibody complexes at the surface of cancer cells, which enhances interactions between the antibody Fc region and immune cell receptors to improve antibody-dependent cell-mediated cytotoxicity (ADCC) and enhances the rate of receptor-antibody internalization and degradation in lysosomes.

To optimize mAbs capable of bioorthogonal clicking, we selected two model click pairs composed of mAbs targeting the human epidermal growth factor receptor 2 (HER2) and epidermal growth factor receptor (EGFR), which are receptors overexpressed in a panel of cancers[25-27]. We optimized the click conjugation ratios by reacting mAbs with *trans*-cyclooctene (TCO) or tetrazine (Tz). The antibodies were conjugated with the TCO or Tz click moieties (containing 4 and 5 polyethylene glycol (PEG) linkers) via *N*-hydroxysuccinimidyl ester (NHS-ester) reactions (**Extended Fig. 1a**). The modification of mAbs with TCO or Tz, did not affect antibody immunoreactivity and stability

(**Supplementary Fig. 1a,b)**. Matrix-assisted laser desorption/ionization time-of-flight (MALDI-TOF) mass spectrometry analyses of the conjugates revealed 10-12 click moieties per mAb (**Extended Fig. 1b,c**).

To elucidate the reaction kinetics of bioorthogonal click between mAbs-TCO (click pair I, **Fig. 1a**) and mAbs-Tz (click pair II, **Fig. 1a**), we performed SDS-PAGE analyses (**Fig. 1b**). The Tz-modified mAbs were fluorescently labeled with indocyanine green (ICG) dye to enable visualization and quantification. As shown in **Fig. 1b**, the click reaction between mAbs-TCO and mAbs-Tz occurred between 30-90 minutes when reacted at equimolar ratios between 1:1 and 1:0.8 of mAbs-TCO:mAbs-Tz. No high molecular weight products were observed at shorter reaction times, indicating minimal intermolecular clicked products formed. To validate the click reaction between antibody-TCO and antibody-Tz in a 1:1 ratio for 90 minutes, control experiments were conducted by adding an excess of unreacted TCO or Tz click moieties, effectively quenching the click reaction (**Supplementary Fig. 1c)**.

Next, to validate that antibody clicking results in antibody dimerization, we performed transmission electron microscopy (TEM) imaging of the pre-clicked mAbs at 1:1 ratio for 90 min (**Fig. 1c**). The TEM images demonstrated formation of mAb dimers upon click reaction between Panitumumab-TCO (Pan-TCO, anti-EGFR mAb) and Trastuzumab-Tz (Trast-Tz, anti-HER2 mAb) (**Fig. 1c**). Overall, these results validate bioorthogonal clicking of TCO- and Tz-modified mAbs, demonstrating formation of covalently linked antibody complexes.

**Bioorthogonal Clicking Augments Antibody Cellular Retention and Tumor Uptake**

Previous studies have shown that antibody combinations result in a large number of antibody-receptor complexes at the cell surface of cancer cells, which enhances the rate of antibody-receptor internalization and degradation in lysosomes[28]. To investigate whether antibody-ADC click enhances mAb internalization, we performed immunofluorescence (IF) studies comparing a panel of clicking mAbs pairs. Control studies included no click mAbs pairs (**Fig. 2a**). IF analyses showed that HER2-positive and EGFR-low ($HER2^+$/EGFR-low) NCIN87 cancer cells (**Supplementary Fig. 1d)** contained higher intensity (~1.4-fold) and colocalization (~3.5-fold) of the clicked anti-HER2/anti-EGFR mAbs compared to the no click mAbs pair (**Fig. 2b**). We also observed higher colocalization of the anti-HER2 clicked mAbs pair targeting distinct epitopes of the HER2 receptor (pertuzumab-TCO plus trastuzumab-Tz) compared to no click mAbs in $HER2^+$/$EGFR^-$ BT474 cancer cells resistant to trastuzumab and CT26 cells stably expressing HER2 (CT26-hHER2 **Supplementary Fig. 1d and Extended Fig. 2a**). Control studies in the CT26 mouse cancer cell line that does not express human HER2 or human EGFR demonstrated low and comparable uptake in both click and no click conditions (**Extended Fig. 2a**). Additional control studies using non-specific IgG-Tz and TCO-conjugated anti-HER2 or anti-EGFR antibodies demonstrated substantial binding of IgG-Tz to cells where anti-EGFR or anti-HER2 mAbs-TCO were attached, in contrast to the no-click conditions (**Supplementary Fig. 1e**). These results in $HER2^+$ and $HER2^+$/EGFR-low cancer cells demonstrate that dual engagement of two distinct receptors or different epitopes of the same receptor *via* bioorthogonal clicking improves mAb uptake when compared to conventional single-receptor binding.

Additional studies in EGFR$^+$ A431 cancer cells that do not express HER2 receptors (HER2$^-$/EGFR$^+$, **Supplementary Fig. 1d**), demonstrated that the click conjugation of anti-HER2-Tz mAbs with anti-EGFR-TCO mAbs enhanced binding of anti-HER2 antibodies (**Extended Fig. 2a**). These results suggest that the anti-EGFR antibody-TCO facilitates the binding of the clicked anti-HER2 mAbs-Tz through the biorthogonal clicking in A431 cells. Altogether, these findings suggest a potential to extend the targeting potential of anti-HER2 mAbs therapy beyond cells that only express HER2, as long as it is clicked to a partnering antibody that recognizes an antigen on the cells of interest.

To further assess the endocytic trafficking of antibody click, we utilized lysosome-associated membrane protein 1 (LAMP1) immunostaining to visualize lysosomes and late endosomes. IF analyses in NCIN87 HER2$^+$/EGFR-low cancer cells revealed significantly higher colocalization of the fluorescently-tagged clicking antibodies with LAMP1-positive vesicles compared to non-clicking mAbs controls (**Fig. 2c**). To visualize antibody endocytic trafficking, we conjugated the click and no click mAbs pairs with the pH-sensitive dye pHrodo (**Fig. 2a**), which increases fluorescence in acidic endosomes. Clicked antibody conjugates showed significantly higher pHrodo intensity over time versus non-clicked antibodies, indicating improved internalization and trafficking to endolysosomes (**Fig. 2d** and (**Extended Fig. 2b**). Additional studies using anti-EGFR mAbs and the anti-HER2 antibody-drug conjugate trastuzumab emtansine (T-DM1)[29] demonstrated an increase in DM1 drug delivery in click conditions when compared with no click (**Fig. 2e**). Overall, these data provide additional evidence that bioorthogonal clicking of antibodies targeting two different receptors or distinct epitopes of the same receptor enhances antibody intracellular delivery compared to traditional single-receptor targeting approaches.

**Antibody-PET Reveals Enhanced Tumor Targeting by Clicking mAbs**

Radiolabeled antibodies combined with positron emission tomography (PET) allow visualization of mAbs distribution and tumor uptake in the whole body[30]. In this study, mAbs were radiolabeled with the positron emitters zirconium-89 ($^{89}$Zr) or copper-64 ($^{64}$Cu) and mAbs-PET followed by biodistribution studies were performed to determine the biodistribution of click versus no click mAbs HER2/EGFR pairs. As outlined in the scheme of **Fig. 3a**, mice bearing HER2+/EGFR-low NCIN87 tumors were administered an intravenous injection of 50 μg of the FDA-approved anti-EGFR antibody Pan-TCO on day 1, followed by injection of 50 μg of the radiolabeled anti-HER2 antibody [$^{89}$Zr]Zr-DFO-Trast-Tz (50 μg; 200 μCi) on day 2. Immuno-PET and biodistribution studies at 48 h after injection of [$^{89}$Zr]Zr-DFO-Trast-Tz (**Fig. 3b,c**) revealed that the biodistribution patterns of the clicking mAb pairs closely aligned with the expected biodistribution profile of antibodies exhibiting tumor uptake (26.4 ± 7.5 %ID/g) and liver clearance (9.9 ± 0.66 %ID/g). These profiles were consistent with the conventional PET and biodistribution characteristics of traditional $^{89}$Zr-labeled antibodies.

In our pilot studies, control studies using IgG-TCO as the click pair I demonstrated low uptake in the tumor (**Supplementary Fig. 2**). Additionally, liver uptake of clicking mAbs was ~3-fold higher when compared with [$^{89}$Zr]Zr-DFO-Trast-Tz no click (**Supplementary Fig. 2**) likely due to bioorthogonal click reaction occurring in blood circulation that results in an enhancement in the interaction of the Fc domain of antibodies with Fc receptors in the liver of immunocompromised mice[31]. Additional studies demonstrated that pre-injection of a 100-fold excess of cold IgG significantly lowered liver accumulation by blocking the Fc-mediated interaction of the antibodies with Fc receptors in liver cells (**Extended Fig. 3a-c**). Interestingly, we observed lower liver uptake of click antibodies in immunocompetent mice (8.9±1.5 %ID/g) when compared with

immunocompromised mice (4.5±2.4 %ID/g), as immunocompetent mice have circulating IgG [31, 32](**Supplementary Fig. 3**).

In addition to determining Pan-TCO/Trast-Tz in HER2$^+$/EGFR-low NCIN87 cancer cells, we also evaluated the clicking of a pair of antibodies that target distinct epitopes of the HER2 receptor. We used Trast and pertuzumab (Per) that bind domains II and IV of HER2 (**Extended Fig. 3a**) [33, 34]. Antibody-PET and biodistribution studies using Trast-TCO or Per-TCO in combination with [$^{89}$Zr]Zr-DFO-Trast-Tz demonstrated similar tumor accumulation compared to [$^{89}$Zr]Zr-DFO-Trast-Tz alone (**Extended Fig. 3c-d**). The Trast-TCO or Per-TCO binding does not result in the blocking of the second click pair *i.e.,* Trast-Tz (**Extended Fig. 3c-d**). On the other hand, tumor uptake of Pan-TCO/Trast-Tz was ~1.5-fold higher when compared with Trast alone, and further studies were conducted with this antibody click pair.

**Antibody click enables uptake of both HER2$^+$ and HER2$^-$ tumors**

We next sought to investigate the potential of the Pan-TCO/Trast-Tz clicking mAb pair in a inter-tumor heterogeneous model. For this, we used a bilateral model where HER2$^+$ (NCIN87) and HER2$^-$ (A431, **Supplementary Fig. 1d**) tumors were xenografted on the right and left shoulder of *nu/nu* mice, respectively (**Fig. 3d**). This model enabled the evaluation of the uptake of the Pan-TCO/Trast-Tz click pair in HER2$^+$ and HER2$^-$ tumors simultaneously in the same animal. An intravenous injection of 50 μg of Pan-TCO was administered on day 1, followed by an injection of 50 μg of the anti-HER2 antibody [$^{64}$Cu]Cu-NOTA-Trast (no click) or click [$^{64}$Cu]Cu-NOTA-Trast-Tz (50 μg; 200 μCi) on day 2. As observed in **Fig. 3d,e**, [$^{64}$Cu]Cu-NOTA-Trast (no click) accumulated in the HER2$^+$ tumor as expected (28.9±3.8 %ID/g) with very low uptake in the HER2$^-$

tumor (3.7±0.6 %ID/g). In the Pan-TCO plus [$^{64}$Cu]Cu-NOTA-Trast-Tz click group, we observed antibody uptake in both HER2$^{+}$ (25.9±3.8 %ID/g) and HER2$^{-}$ tumors (15.2±2.9 %ID/g). The uptake in the A431 HER2$^{-}$ tumors was a result of [$^{64}$Cu]Cu-NOTA-Trast-Tz clicking with Pan-TCO bound to EGFR receptors in these tumors. To further validate that a TCO/Tz approach of antibody click enables delivery of antibodies regardless of HER2 antigen presence, we performed additional studies using Pan-TCO or Trast-TCO followed by bioorthogonal clicking with [$^{64}$Cu]Cu-NOTA-IgG-Tz (**Extended Fig. 4**). As predicted, antibody click occurred predominantly in tumors pre-bound by the first click mAbs, validating the target-directed nature of this approach. Overall, antibody bioorthogonal click chemistry enables imaging of both HER2$^{+}$ and HER2$^{-}$ tumors, exceeding the imaging capabilities of conventional single-receptor targeting radiolabeled anti-HER2 antibodies (**Fig. 3e,f**).

**Antibody-ADC Click Enhances Efficacy and T-Cell Recruitment in Tumors**

Given the enhanced tumor accumulation and internalization of antibody click when compared with the conventional no click approaches (**Figs. 1-3**), we sought to perform therapeutic studies evaluating the efficacy of antibody-ADC click. The anti-HER2 ADC trastuzumab derutexan (T-DXd)[29] has garnered significant recent attention due to its exceptional clinical efficacy in targeting cancer cells with potent payloads. Therefore, T-DXd was used in our therapeutic studies as the ADC-Tz click pair. First, we validated the cytotoxic potency of antibody-TCO/ADC-Tz click *in vitro* using cancer cell lines expressing varying levels of HER2 and EGFR (**Supplementary Fig. 1d**). The 50% inhibitory concentration ($IC_{50}$) values of T-DXd in HER2$^{+}$ NCIN87 and HER2$^{-}$ A431 cancer cells were 17-fold and 4-fold lower, respectively, for antibody-ADC click when compared

with no click control (**Extended Fig. 5**). The results obtained in cell death assays were consistent with enhanced intracellular ADC delivery as observed in our cell studies (**Fig. 2**).

We next validated antibody-ADC click efficacy *in vivo* using HER2$^{+}$/EGFR-low NCIN87 tumor-bearing mice. Administration of Pan-TCO plus T-DXd-Tz (click) at a clinically relevant dose of 10 mg kg$^{-1}$ [35, 36] resulted in enhanced reduction of NCIN87 tumor growth compared to treatment with Pan/T-DXd (no click) or T-DXd alone (**Supplementary Fig. 4**). In subsequent therapeutic studies, we reduced T-DXd dose from 10 mg kg$^{-1}$ to a single dose of 5 mg kg$^{-1}$ with the aim to determine feasibility of T-DXd dose reduction in click approaches while mitigating possible ADC-related side effects.

T-DXd shows clinical benefit in patients with HER2-high and HER2-low tumors[37], but most of patients will ultimately experience disease progression. Additionally, T-DXd does not accumulate in high levels in non-expressing HER2 cancer cells[38]. To determine if antibody-ADC click could extend the potential benefit of T-DXd to non-expressing HER2 tumors, we performed therapeutic studies in a bilateral model of HER2$^{+}$ NCIN87 and HER2$^{-}$ A431 cancer cells (**Fig. 4a** and **Supplementary Fig. 5**). Mice received an intravenous injection of Pan or T-DXd (5 mg kg$^{-1}$ once) alone or in combination. The vehicle and Pan cohorts had a similar trend of increased tumor volume over time. T-DXd alone inhibited tumor growth in HER2$^{+}$ tumors, but HER2-negative tumors did not respond. The combination of Pan with T-DXd (no click) slightly decreased tumor volume in HER2$^{-}$ tumors, when compared with T-DXd monotherapy, but tumor ulceration, was observed at 34 days after therapy. Mice receiving a combination of Pan-TCO and T-DXd-Tz (click, both at 5 mg kg$^{-1}$), showed complete remission of the HER2$^{+}$ tumors in 80% of total treated mice. Among all the tested groups in HER2$^{-}$ tumors, the Pan-TCO/T-DXd-Tz click group exhibited the

most potent inhibition of tumor growth. Additionally, the T-DXd click led to enhanced survival compared to both T-DXd alone or in combination with Pan (no click) (**Supplementary Fig.5**). These results further demonstrate the potential of antibody-ADC click to augment ADC efficacy against tumors of heterogeneous expression to the targeted antigen.

In addition to NCIN87 xenografts, we evaluated antibody-ADC click therapy in immunocompetent mice bearing CT26-hHER2 (**Supplementary Fig. 1d**). When mice with CT26-hHER2 were treated with vehicle, 5 mg $kg^{-1}$ anti-HER2 (Per), T-DXd, or a combination of Per plus T-DXd (no click), the mean of tumor volumes at day 12 days post-therapy were ~3200, 2700, 2800, 2800 $mm^3$, respectively (**Fig. 4b**). A complete response was observed in 60% (6/10) of mice who received the Per-TCO/T-DXd-Tz click treatment. Subsequently, these successfully treated mice were subjected to rechallenge with CT26-hHER2 cancer cells, resulting in the complete rejection of the cancer cells in the rechallenged mice (**Fig. 4c**). In CT26-hHER2 tumors subjected to click therapy, a notable ~3.6 and 1.5-fold increase in the accumulation of $CD8^+$ T cells within the tumors was observed by CD8-targeting immunoPET, in contrast to the vehicle or non-click-treated groups (**Fig. 4d,e**). Additional *in vitro* studies using peripheral blood mononuclear cells from a healthy donor validated the CD8 PET imaging studies showing an increase in ADCC in antibody-ADC click when compared with no click (**Supplementary Fig. 6**). These results suggest that antibody-ADC click strategies using the anti-HER2 T-DXd ADC result in enhanced intracellular drug delivery, potent ADC cytotoxicity in both $HER2^+$ and $HER2^-$ tumors, and antitumor memory response in heterogeneous tumor models.

**Bioorthogonal Antibody-ADC Click Enables Efficacy Against Unresponsive or Drug-Resistant Tumors**

Having validated augmented ADC accumulation *via* bioorthogonal antibody-ADC click, we next evaluated efficacy in cancer models unresponsive or resistant to ADC therapy. First, mice bearing HER2$^{+}$/EGFR-low NCIN87 xenografts were administered T-DXd monotherapy. At 30 days after therapy, mice were divided into T-DXd responders (fold-change in tumor volume equal to or lower than 1) and non-responders (fold-change in tumor volume higher than 1) as shown in **Fig. 5a** and (**Supplementary Fig. 7a**). HER2-targeting immuno-PET studies using [$^{64}$Cu]Cu-NOTA-Trast demonstrated a reduction in HER2 expression in both T-DXd responder and non-responder tumors as observed by immunoPET (**Fig. 5b** and **Supplementary Fig. 7b**). Prior clinical data demonstrated EGFR upregulation as a resistance mechanism to HER2-targeted therapies[27], and we, therefore, assessed the EGFR protein levels in tumors that exhibited non-responsiveness to T-DXD. Western blot studies showed an increase in EGFR total protein levels in the non-responder T-DXd treated tumors when compared with responders (**Fig. 5c**). After stratification in ADC responders versus non-responders, the responsive cohorts remained on T-DXd monotherapy, while the non-responsive mice were switched to a combination of anti-EGFR Pan-TCO plus T-DXd-Tz click therapy. Notably, antibody-ADC click therapy resulted in enhanced tumor growth suppression in previously non-responsive tumors compared to mice that continued to receive ADC monotherapy. In cohorts treated with no click ADC, tumors transitioned from responsive to unresponsive tumors (**Fig. 5d**). In this study, we observed a trend suggesting an improved therapeutic response to click therapy in male mice when compared to female mice. However, statistical analysis revealed that the observed difference between the sexes did not attain statistical significance (**Supplementary Fig. 7c**).

To further confirm the potential of antibody-ADC click therapy to treat resistant tumors, we validated click efficacy in a BT474 trastuzumab-resistant cancer model (**Fig. 5e**). Mice inoculated with trastuzumab-resistant BT474 tumors were treated with T-DXd alone and stratified as responder or non-responders based on their tumor volume (**Fig. 5e** and **Supplementary Fig. 7d**). Five out of 6 mice bearing BT474-trastuzumab resistant tumors demonstrated to be non-responders to T-DXd. Non-responder mice were then switched to a combination of anti-HER2 Per-TCO and T-DXd-Tz click for dual HER2 targeting. Upon switching BT474 tumors that exhibited resistance to both trastuzumab and T-DXd, to an antibody-ADC click therapy, the bioorthogonally clicked antibody-ADC pair demonstrated effective tumor suppression (**Fig. 5f)**. These results demonstrate that a strategy of dual targeting through antibody-ADC click effectively overcomes drug resistance, further validating the potential of this approach to enhance outcomes in refractory cancers.

## METHODS

### Ethical compliance

Animal studies were performed in the Washington University School of Medicine animal facility in compliance with institutional guidelines under Institutional Animal Care and Use Committee (IACUC) approved protocols (Animal Protocol 21-0087, IBC protocol 13652, PI: Pereira).

### Cell culture

Human cancer cell lines NCIN87, A431, BT474, and CT26 were purchased from the American Type Culture Collection (ATCC). All cell lines used were mycoplasma-free and cultured at 37 °C in a humidified atmosphere at 5% $CO_2$. All cell culture media were supplemented with 100 units $mL^{-1}$ penicillin and streptomycin. Details of cell culture media for respective cell lines are detailed in **Supplementary Table 1**.

*Generation of CT26 murine cancer cells stably expressing human HER2 (CT26-hHER2)*

We used our previously reported methods to develop the CT26-hHER2 cell line[40]. Briefly, we transduced the murine cancer cell line CT26 using 8 g $mL^{-1}$ hexadimethrine bromide (Sigma) and the media was changed 24 h later. A puromycin selection (5 μg $mL^{-1}$) was initiated 3 days after the transduction, and was continued for a minimum of 4 days after that. Western blot analysis confirmed the increase in human HER2 expression in the CT26 cells (**Supplementary Fig. 1d**), and *ex vivo* biodistribution analysis confirmed the expression of HER2 in CT26-hHER2 cells implanted in the mouse (**Supplementary Fig. 3**).

*Generation of BT474 cancer cells resistant to trastuzumab (BT474-trastuzumab resistant)*

BT474 human breast cancer cells were made resistant to trastuzumab by continually exposing the parental BT474 cancer cells to increasing concentrations (up to 15 μg $mL^{-1}$) of the trastuzumab antibody over a period of 9 months. The development of resistance was confirmed by viability assays.

**Antibody modification and characterization**

*Antibody modification*

Antibodies — Panitumumab (Pan), Pertuzumab (Per), Trastuzumab (trast), IgG, T-DM1 and T-DXd (**Supplementary Table 2**) — were conjugated at a molar ratio of 15 TCO-$(PEG)_4$-NHS-ester (TCO) (*i.e.*, TCO) or Tz-$(PEG)_5$-NHS-ester (Tz) (*i.e.*, Tz) per mAb. All conjugation reactions were carried out in an amine-free solution (PBS, pH 8.8-9) at 37 °C with 450 rpm agitation for 1 h. Additionally, the unconjugated chemical TCO/Tz click moieties were removed from the conjugated antibodies using a size exclusion column (PD-10; GE Healthcare). The conjugate solutions were further concentrated using amicon filters with a 50 kDa cutoff.

For immunofluorescence (IF) studies, the TCO- or Tz-conjugated mAbs were then labeled with Alexa Fluor 488 (Thermo Fisher Scientific, A2042), Alexa Fluor 594 (Thermo Fisher Scientific, A20004), pH-Rhodo (Thermo Fisher Scientific, P36600), or indocyanine green (ICG) at a molar ratio of 3 fluorophores per mAbs at 37°C in PBS at pH 8.8. The fluorescently-labeled mAb conjugates were purified via size exclusion chromatography (PD-10 column; GE Healthcare) and concentrated using 50KDa cutoff amicon filters.

The concentration of the antibody conjugates was determined by measuring absorption using a UV-visible spectrophotometer, Pierce 660 assay (Thermo Fisher Scientific, 22660), or BCA assay (Thermo Fisher Scientific, 23227). All antibody conjugates were stored at -80 °C protected from light until used.

*SDS-PAGE gels*

Pan-TCO and Trast-Tz-ICG were incubated at different ratios (1:1, 1:0.8, 1:0.6, 1:0.4 and 1:0.2), respectively, for 90 min at 37 °C with 450 rpm agitation. Additional experiments were conducted in 1:1 reaction ratios at different incubation times (90, 30, 10 and 1 min) at 37 °C with 450 rpm agitation. Then, the samples were mixed with loading buffer and boiled under reducing conditions (Laemmli buffer, Invitrogen) for 5 min at 95 °C, and loaded onto SDS-PAGE gels (NuPage 4-12% Bis-Tris protein gels, Invitrogen).

To perform blocking experiments, mAbs conjugated to trans-cyclooctene (mAbs-TCO) or tetrazine (mAbs-Tz) were pre-incubated with a 100-fold molar excess of unconjugated Tz or TCO, respectively. Pre-incubation was performed for 90 minutes at 37°C with 450 rpm agitation. After pre-incubation, the clicking pair of mAbs (mAbs-Tz or mAbs-TCO) was added in a 1:1 molar ratio of conjugated antibodies. The degree of click conjugation was then compared to a positive control with no blocking (clicked mAbs) and a negative control with no click moieties (unconjugated mAbs). After SDS-PAGE, the gels were rinsed with deionized water, stained with Pierce Mini Gel Power Staining and Destaining Kit, and scanned on the Odyssey CLX.

*MALDI spectrometry and TEM*

Matrix-assisted laser desorption/ionization-time of flight (MALDI-TOF) mass spectrometry of the antibody conjugates was performed to determine the number of conjugates per antibody. TEM of the unconjugated and conjugated antibodies was performed by the Alberta Proteomics and Mass Spectrometry Facility (Centre For Pharmacy and Health Research Building (KGR)) at University of Alberta in Canada.

**Immunofluorescence**

Cancer cells (1 million cells) grown on coverslips of 1.5 mm thickness ( ThermoFisher Scientific, 12-542B) were incubated with 100 nM of Alexa Fluor 488 tagged mAbs-TCO reconstituted in PBS containing 1% BSA and incubated for 30 min at 4 °C with gentle agitation. Next, cells were washed to remove unbound mAbs and incubated with 100 nM of mAbs-Tz tagged with Alexa-Fluor 594 or pHrodo for 3, 24 or 48 h at 37 °C in 5% $CO_2$. Control experiments included unconjugated mAbs tagged with Alexa Fluor 488 or Alexa Fluor 594.

Experiments of LAMP-1 staining were performed after cells fixation with 4% paraformaldehyde (PFA) and permeabilization with PBS containing 1% Triton X-100, followed by incubation with a rabbit anti-LAMP-1 primary mAb (ab24170, Abcam) and secondary goat anti-rabbit IgG fluorescently labeled with Alexa Fluor 488 (A-11008, ThermoFisher Scientific). Fluorescence images were acquired using a 60X oil immersion objective on the EVOS M5000 Imaging microscope.

**pHrodo-internalization assays**

Cells were plated in a 96-well plate (10,000 cells/well). Twenty-four hours after plating, cells were incubated with mAbs-TCO-Alexa Flour 488 or mAbs- Alexa Flour 488 (100 nM) in 1% BSA in PBS for 30 min at 37 °C, followed by washing using ice-cold PBS. Later, cells were incubated with mAbs-Alexa Flour 594 or mAbs-Tz -Alexa Flour 594 or mAbs-pHrodo or mAbs-Tz-pHrodo (100 nM) at 37 °C and 5% $CO_2$ for 3 h, 24 h and 48 h. At the time of fluorescence measurement, the cells were washed 5 times using ice-cold PBS and fluorescence measurements were recorded using Synergy H1 microplate reader (Biotek).

**Cell viability assays**

Cancer cells (20,000 cells/well: NCIN87, A431, CT26-hHER2, CT26, BT474 cells) were plated on a 96-well plate for 24 h. In no click conditions, the cells were incubated on ice with Pan, Trast or Per alone during 30 min. Next, cancer cells were washed 3 times using ice-cold PBS. Later, cancer cells were treated with T-DXd during 48 h. In antibody-ADC click treatment groups, the cancer cells were treated with TCO modified mAbs (Pan-TCO, Per-TCO, or Trast-TCO) for 30 min on ice. After washing cells during 3 times using ice-cold PBS, the cells were treated during 48 h with T-DXd drugs modified with Tz (T-Dxd-Tz). Antibody concentrations were tested at 100, 10, 1, 0.1, 0.01, and 0.001 nM and at a molar ratio of 1:1 in all click and no click conditions. After 48 h of incubation with the no click or click pairs, a media change was performed, followed by the addition of 20 μL of a mixture of WST-8 (1.5 mg $mL^{-1}$, Cayman Chemical) and 1-methoxy-5-methylphenazinium methylsulfate (100 μM, Cayman Chemical) per manufacturer's instructions.

Next, the plates were incubated for 2 h in a $CO_2$ incubator with gentle agitation, and absorbance in each well was measured at 460 nm.

***In vitro* quantification of ADC by ELISA assay**

Cells were plated on six-well plates (2 million cells /well). After 24 h, the cells were treated with no click or click pair of mAbs. The mAbs or mAbs-TCO (100 nM) was incubated on ice for 30 min followed by washing using ice-cold PBS. Later, the T-DM1 or T-DM1-Tz (100 nM) were added to the cells on ice for 30 min under shaking conditions followed by incubation at 37 °C and 5% $CO_2$ for 48 h. Samples were prepared for the DM1 ELISA assay as instructed by the manufacturer (Eagle Biosciences, KTR-756).

***In vitro* analysis of antibody-dependent cellular cytotoxicity (ADCC) experiments**

Cells were plated on 96 well plates (20,000 cells/well). After 24 h, the cells were treated with no click or click pair of mAbs. The first mAbs or mAbs-TCO (100 nM) was incubated on ice for 30 min followed by washing using ice-cold PBS. Then Trast or Trast-Tz (100 nM) were added to the cells on ice for 30 min under shaking conditions. Later, the PBMCs (one million PBMCs/well) were added to achieve a ratio of 1:50 (*i.e.*, cancer cells: PBMCs) followed by incubation at 37 °C / 5% $CO_2$ for 48 h. For blocking cohorts, half a million of PBMCs were pre-incubated with 0.5 mg of IgG (Human isotope) for 1 h on ice, before culturing the PBMCs with cancer cells. ADCC in no click or click mAbs was evaluated using the Cytotoxicity Detection Kit (LDH, Roche) as instructed by the manufacturer.

**Western blot analyses**

Western blot of tumor and cell lysates were performed using our previously reported methods[40, 41]. Primary antibodies used in this study included rabbit anti-HER2, 1:800 (ab131490; Abcam); rabbit anti-EGFR, 1:1,000 (ab52894; Abcam), and mouse anti β-actin, 1:10,000 (A1978; Sigma). After incubation with the primary mAbs, membranes were washed with TBST buffer for three times with gentle agitation and incubated with secondary antibodies (anti-mouse goat IgG conjugated with AlexaFluor Plus 800 or anti-rabbit goat IgG conjugated with AlexaFluor 680, Invitrogen) for 1 h at room temperature. Membranes were scanned using the Odyssey infrared imaging system (LI-COR Biosciences).

**Radiolabeling and binding assays**

*[$^{89}$Zr]Zr-DFO-Antibody-Tz*

$^{89}$Zr-oxalate used in the studies was purchased from the WUSTL Isotope Production Team. Antibodies were conjugated with *p*-isothiocyanatobenzyl-desferrioxamine (DFO-Bz-NCS; Macrocyclics, Inc) at a molar ratio of 5 DFO per antibody at a pH of 8.8 (37°C, 450 rpm agitation). The unconjugated DFO was removed from the antibody-DFO conjugates using a size exclusion column (PD-10; GE Healthcare) and the antibody solutions were concentrated using amicon filters with a 50 kDa cutoff filter. The purified antibody-DFO was then reacted with Tz at a molar ratio of 15 tetrazine-$(PEG)_5$-NHS per mAb at a pH 8.8 (37°C, 450 rpm agitation). Subsequently, the mAbs-DFO-Tz was purified using the size exclusion PD10 column in the chelex PBS, followed by amicon cleaning. After confirming mAb conjugation and clicking efficacy by SDS-PAGE and

MALDI, mAbs-DFO-Tz was labeled with zirconium-89 at a pH 7.4 for 60 min at 37°C. [$^{89}$Zr]Zr-DFO-mAbs-Tz used in the study had a radiochemical yield and purity above ~95% respectively.

*[$^{64}$Cu]Cu-NOTA-Antibody-Tz*

We purchased Copper-64 from the WUSTL Isotope Production Team. First, mAbs were buffer exchanged and concentrated in 0.1 M 4-(2-hydroxyethyl)-1-piperazineethanesulfonic acid (HEPES) buffer (pH 8.5). The purified mAbs was then reacted with a 20-fold molar excess of 2-S-(4-Isothiocyanatobenzyl)-1,4,7-triazacyclononane-1,4,7-triacetic acid (*p*-SCN-Bn-NOTA, Macrocyclics) overnight at 4 °C with gentle agitation. Afterwards, the NOTA modified mAbs were purified and buffer exchanged using PD10 columns in PBS (pH 7.4), followed by amicon filtration with a 50 kDa cutoff filter. mAbs-NOTA was then reacted with tetrazine-$(PEG)_5$-NHS ester at a molar ratio of 15 per mAbs for 1 h at 37 °C with 450 rpm agitation. Additionally, the unconjugated NOTA was removed using a size exclusion column (PD-10; GE Healthcare) and the antibody solutions were concentrated in ammonium acetate buffer (pH 5.5) using amicon filters with a 50 kDa cutoff. The efficacy of mAbs to click or the presence of any aggregation was validated by performing SDS-PAGE followed by Coomassie staining. Later, mAbs-NOTA-Tz was reacted with $^{64}$Cu for 1 h at 37 °C with 450 rpm agitation. A mixture of 50 mM ethylenediaminetetraacetic acid (EDTA) and methanol was used in iTLC to determine a radiochemical yield of ~95% and radiochemical purity of ~98%, respectively.

*Total binding assays*

For total binding assays, 1 million cancer cells, were incubated in PBS containing 1% w/v bovine serum albumin (BSA, Sigma Aldrich) and 0.1% w/v sodium azide ($NaN_3$, Sigma Aldrich) in the

presence 2.5 μg of Pan-TCO or Per-TCO or Trast-TCO on ice for 30 min at 450 rpm. Later, the cells were centrifuged at 1500 rpm for 5 min at 4°C to remove unbound mAbs. Next, the cells were resuspended in PBS containing 1% w/v BSA and 0.1% w/v sodium azide. The radiolabeled antibodies (2.5 μg) [$^{89}$Zr]Zr-DFO-Trast or [$^{89}$Zr]Zr-DFO-Trast-Tz or [$^{89}$Zr]Zr-DFO-IgG-Tz were added to the cancer cells and incubated on ice during 90 min at 37 °C. PBS containing unbound radioimmunoconjugates was removed by centrifuging cells at 1500 rpm for 5 min at 4°C. The previous centrifugation steps were repeated three times and the activity bound to the cell pellet was measured on a gamma counter calibrated for $^{89}$Zr. The percent bound activity was calculated by dividing the cell pellet activity to the total activity in the suspension and cell pellet.

**Small animal PET imaging and biodistribution studies**

Mice were first injected with TCO-conjugated antibody (50 $\mu$g). At 24 h after injection of the TCO-conjugated antibody, mice were injected with [$^{89}$Zr]Zr-DFO-mAbs or [$^{64}$Cu]Cu-NOTA-mAbs and used for both biodistribution and PET imaging studies. Acute biodistribution and PET imaging studies were performed at 24 h or 48 h after tail vein injection of the [$^{89}$Zr]Zr-DFO-mAbs or [$^{64}$Cu]Cu-NOTA-mAbs, respectively.

Mice used for biodistribution studies were sacrificed and organs were harvested, weighed, and assayed in a gamma counter. The radioactivity was expressed in each organ as a percentage of the injected dose per gram of the organ (%ID/g).

PET imaging was conducted on a on a Mediso nanoScan PET/CT scanner (Mediso) at 24 h or 48 h post-injection of [$^{89}$Zr]Zr-DFO-mAbs or [$^{64}$Cu]Cu-NOTA-mAbs modified with or without Tz. The mice were anesthetized by inhalation of 2% isofluorane (Baxter Healthcare) in an oxygen gas mixture before recording PET-CT images. PET data for each group (n = 3) was recorded. Images

were analyzed using 3D Slicer software (version 5.0.3, a free and open source software https://www.slicer.org/)).

*$CD8^+$ T-cell imaging*

CT26-hHER2 xenografts with a volume of ~200 $mm^3$, were randomly divided them into control, no click and click groups. The mice in the control cohort received saline injection. In the no click and click groups, mice received the Per or Per-TCO (5 mg $kg^{-1}$) injections on day 1. On day 2, mice in the no click or click groups received T-DXd or T-DXd-Tz (5 mg $kg^{-1}$) injections. On day 3, [$^{64}$Cu]Cu-NOTA-Anti-mouse CD8 mAbs (2.5 mg $kg^{-1}$, ~7.4 Mbq) was intravenously injected in mice in the control, no click or click groups. The mice were then imaged at 24 and 48 h timepoints using the Mediso PET Scanner. The mice were anesthetized by inhalation of 2% isofluorane (Baxter Healthcare) in an oxygen gas mixture before recording PET-CT images. PET data for each group ($n = 3$) was recorded. Image analyses and regions of interest (ROI) quantifications were done using 3D Slicer software (version 5.0.3, a free and open source software https://www.slicer.org/)).

***In vivo* therapeutic efficacy studies**

All animal experiments were conducted in accordance with guidelines approved by Washington University School of Medicine's Research Animal Resource Center and Institutional Animal Care and Use Committee. Eight- to 10-week-old *nu/nu* female or male mice and 4 to 6-week-old Balb/c female or male mice were obtained from Charles River Laboratories. The therapies were initiated when the tumor volume reached ~200 $mm^3$ and tumor volume was measured twice a week by

caliper measurements. Humane endpoints were defined as tumor volumes > 1,500 $mm^3$, bodyweight loss of >20%, tumor ulceration, and other clinical symptoms of acute toxicity. At the terminal stage, tumors were collected for the western blot analysis.

*$HER2^+$ gastric cancer model*

Mice bearing $HER2^+$ NCIN87 xenografts were stratified into the following groups: control (saline), Panitumumab (Pan), T-DXd, no click (Panitumumab plus T-DXd) and click (Pan-TCO plus T-DXd-Tz)cohort. Pan-TCO or Pan was administered at 10 mg $kg^{-1}$ *via* tail vein. At 24 h post-injection of Pan-TCO, the mice received an intravenous injection of T-DXd or T-DXd-Tz (10 mg $kg^{-1}$). Mice in Pan or T-DXd cohorts received intravenous injection of Pan or T-DXd (10 mg $kg^{-1}$) alone.

*$HER2^+$/$HER2^-$ bilateral tumor model*

*Nu/nu* female or male mice (Charles River Laboratories) were injected subcutaneously with 5 million NCIN87 cells, and/or 0.25 million A431 cells in a 100 μL cell suspension of a 1:1 (v/v) mixture of medium with reconstituted basement membrane (BD Matrigel, BD Biosciences). Mice-bearing NCIN87/A431 bilateral tumors were developed by subcutaneous injection of NCIN87 and A431 cancer cells on the bilateral dorsal flank regions. When the tumor volume reached the size of 200 $mm^3$, mice were randomized them into six cohorts: control (saline), Pan (5 mg $kg^{-1}$), ADC alone (5 mg $kg^{-1}$), no click (Pan plus T-DXd, 5 mg $kg^{-1}$), and click (Pan-TCO plus T-DXd-Tz, 5 mg $kg^{-1}$).

*NCIN87 gastric cancer model of acquired resistance to ADC*

*Nu/nu male and female* mice bearing NCIN87 xenografts were treated with T-DXd monotherapy intravenously (5 mg $kg^{-1}$). Nearly one month after therapy, mice were stratified into responders *versus* non-responders, based on the tumor volume measurements, western blot analyses, and HER2-PET imaging. HER2-targeting immuno-PET was performed at 24 h post-intravenous injection of [$^{64}$Cu]Cu-NOTA-trastuzumab (50 $\mu$g, 200$\mu$Ci). The mice that initially did not respond to T-DXd therapy (*i.e.*, non responder) were treated intravenously with Pan-TCO (5 mg $kg^{-1}$) on day 1 and T-DXd-Tz on day 2 (5 mg $kg^{-1}$ as described above), while the responders continued to receive T-DXd therapy (5 mg $kg^{-1}$).

*BT474-trastuzumab resistant model*

*Nu/nu* female mice were implanted subcutaneously with one million BT474-trastuzumab resistant cells. Drinking water of mice receiving estrogen receptor-positive cells BT474 was supplemented with 0.67 μg $mL^{-1}$ of β-estradiol (Sigma) from 1 week in advance of tumor inoculation until mice were sacrificed. Fresh-estradiol supplemented water was provided twice a week. The T-DXd (*i.e.*, ADC) therapy was initiated when the tumor volume reached 200 $mm^3$. The tumor volumes were measured twice a week for a period of ~1 month. Mice were then stratified into responders versus non-responders, based on the tumor volume measurements. The responder mice were maintained on T-DXd (5 mg $kg^{-1}$) therapy and non-responder mice on the click therapy. In the click therapy cohort, the mice were injected with Per-TCO mAbs (5 mg $kg^{-1}$) on day 1. Following this, the mice were injected with T-DXd-Tz (5 mg $kg^{-1}$) on day 2 and tumor volumes were measured twice a week.

*Immunocompetent CT26-hHER2 model*

CT26-hHER2 cancer cells (0.25 million) were xenografted on the right shoulder of the BALB/c mice and treatments were initiated when the tumor volumes reached the size of 200-500 $mm^3$. Then, mice were randomized into six cohorts: control (saline), Per (5 mg $kg^{-1}$), T-DXd (5 mg $kg^{-1}$), no click (Per plus T-DXd, 5 mg $kg^{-1}$), and click (Per-TCO plus T-DXd-Tz, 5 mg $kg^{-1}$). The mice that showed complete remission of the tumors after the therapy, were further rechallenged with 5 million of CT26-hHER2 cancer cells.

**Statistical analyses**

Data were analyzed using GraphPad Prism software version 10.00 (www.graphpad.com). Statistical comparisons of mean values between experimental groups were performed using analysis of variance (ANOVA) followed by Student's t-tests. A *P*-value less than 0.05 was considered statistically significant.

## FIGURE LEGENDS

**Figure 1. Click mAbs enable dual receptor targeting. (a)** Schematic representation of antibodies (mAbs) cross-clicking on the surface of cancer cells. Clicking mAbs enables dual receptor targeting, enhancing drug delivery and tumor-immune cell interaction. **(b)** SDS-PAGE analyses and quantification of the clicking antibodies at a 1:1 ratio over different incubation times, and different ratios at 90 min. **(c)** Cryo-Transmission Electron Microscopy (TEM) images of the mAbs and clicking mAbs. Clicking mAbs were prepared by reacting mAbs-TCO and mAbs-Tz in a 1:1 ratio for 90 min, followed by a negative staining technique for TEM analysis.

**Figure 2. Click mAbs enhance drug delivery in cancer cells. (a)** Schematic representation of mAbs conjugated with TCO, Tz, Alexa-488, Alexa-594, and pHrodo. **(b)** Immunofluorescence analysis of the click mAbs *versus* no click mAbs by fluorescence microscopy. The fluorescence intensity was obtained by quantitative analysis of the NCIN87 cancer cells cultured on 96 well plates. The cells were treated with mAbs or mAbs-TCO conjugated with Alexa-488 fluorophor (100 nM) for 30 min on ice, followed by washing and incubation with Alexa-594 conjugated mAbs or mAbs-Tz (100 nM) for 60 min. Quantitative analysis of the co-localized vesicles in the no click and click groups (n=10). **(c)** Fluorescence microscopy images of the no click and click groups with fluorescently labeled mAbs and LAMP1 in NCIN87 cancer cells, respectively. The first pair of the mAbs or mAbs-TCO (100 nM) was incubated for 30 min at 4 $^{O}$C. Later, after washing, the mAbs-Alexa-594 or mAbs-Tz-Alexa-594 (100 nM) was added to the cells and incubated for 60 min at 37$^{O}$C, followed by LAMP staining. **(d)** Fluorescence microscopy images of the no click and click groups with mAbs labelled with the pH sensitive dye pHrodo which fluoresces upon

internalization. The first pair of the mAbs-Alexa-488 or mAbs-TCO-Alexa-488 (100 nM) was incubated for 30 min at 4 $^{O}$C. Later, after washing, the mAbs-Tz-pHrodo (100 nM) was added to the cells and incubated for 60 min at 37$^{O}$C. Quantitative analysis of the pHrodo fluorescence of the NCIN87 cells treated with 100 nM of the first pair of mAbs or mAbs-TCO for 30 min at 4 $^{O}$C. Later, the cells were washed following the incubation for 60 min at 37$^{O}$C. Fluorescence emission was measured at 3, 24, and 48 h timepoint. **(e)** Quantitative analysis of the T-DM1 ADC internalization in the cells treated with no click and click mAbs at 48 h timepoint using a commercially available ELISA kit.

**Figure 3. Click mAbs enable antibody accumulation in HER2$^{+}$ and HER2$^{-}$ tumors. (a)** Schematic representation of the click PET imaging in the NCIN87 gastric cancer model (HER2$^{+}$/EGFR-low). The first pair of the clicking antibodies *i.e.*, Pan-TCO was injected via the tail vein 24 h prior to the [$^{89}$Zr]Zr-DFO-Trast-Tz and imaged at 48 h post injection. **(b)** Representative PET maximum intensity projection (MIPs) image of the mice bearing the NCIN87 (HER2$^{+}$/EGFR-low) tumor injected with the clicking antibodies and imaged at 48 h timepoint (n=3). **(c)** Biodistribution data at 48 h post-injection of clicking mAbs. The first pair of the clicking antibodies *i.e.*, Pan-TCO (50 $\mu$g) was injected via the tail vein 24 h prior to the [$^{89}$Zr]Zr-DFO-Trast-Tz (50 $\mu$g, ~7.4 Mbq) and biodistribution at 48 h post injection. Bars, n=3 mice per group, mean ± S.E.M. %ID g$^{-1}$, percentage of injected dose per gram. **(d-e)** Representative PET MIPs image of a bilateral tumor model: NCIN87 tumors (HER2$^{+}$/EGFR-low) on the right flank and A431 tumors (HER2$^{-}$/EGFR$^{+}$) tumors on the left flank. The first pair of click antibodies *i.e.,* Pan-TCO or Trast-TCO was injected *via* the tail vein 24 h prior to the injection of [$^{64}$Cu]Cu-NOTA-Trast-Tz (50 $\mu$g, ~7.4 Mbq). All the mice were imaged at 24 h timepoint followed by a

biodistribution study. Bars, n=3 mice per group, mean ± S.E.M. %ID $g^{-1}$, percentage of injected dose per gram. The statically significant differences between experimental groups were performed using analysis of variance (ANOVA) followed by Student's T-test. **(f)** Schematic representation of the conventional PET diagnosis versus the click-PET. Conventional PET allows imaging of one receptor at a time whereas antibody-click PET allows imaging of different receptors expressed in the same tumor or in tumors incolulated in different parts of the living subject.

**Figure 4. Click mAbs enable therapy of HER2$^+$ and HER2$^-$ tumors. (a)** Schematic of a bilateral tumor model where NCIN87 (HER2$^+$) and A431 (HER2$^-$) cancer cells were xenografted on the right and left shoulder, respectively. Mice bearing HER2$^+$/HER2$^-$ bilateral tumors were stratified into different cohorts saline, Pan, T-DXd, no click (Pan plus T-DXd), and antibody-ADC click (Pan-TCO + T-DXd-Tz). A single dose of intravenous injection of each antibody was started at day 0. For the mice receiving the combination of drugs, the first pair of click antibodies *i.e.,* Pan or Pan-TCO (5 mg $kg^{-1}$) was injected *via* the tail vein 24 h prior to the injection of T-DXd or T-DXd-Tz (5 mg $kg^{-1}$). Antibody click significantly improved the treatment of HER2$^+$ tumors and controlled the aggressiveness of HER2$^-$ tumors, resulting in an improvement in the mean survival probability. Bars, n=5 mice per group, mean ± standard error. **(b)** *In vivo* therapeutic efficacy of different cohorts (*i.e.,* control saline, Per, no click (Per + T-Dxd) and antibody-ADC click (Per-TCO plus T-DXd-Tz) validated in immunocompetent mice (BALB/c) bearing CT26-hHER2 tumors. A single dose of intravenous injection of each antibody was started at day 0. For the mice receiving the combination of antibodies, the first antibody click pair *i.e.,* Per or Per-TCO (5 mg $kg^{-1}$) was injected *via* the tail vein 24 h prior to the injection of T-DXd or T-DXd-Tz (5 mg $kg^{-1}$). **(c)** Rechallenging of mice with complete tumor remission after antibody-ADC click therapy

performed by xenografting the 5 million CT26-hHER2 cells on the left shoulder (n=6). **(d-e)** CD8-targeted PET imaging of tumor-infiltrating T cells in mice treated with the click and no click therapy. Scheme represents the mice receiving the combination of drugs, the first pair of click antibodies *i.e.,* Per or Per-TCO (5 mg $kg^{-1}$) was injected *via* the tail vein 24 h prior to the injection of T-DXd or T-DXd-Tz (5 mg $kg^{-1}$), whereas control received saline intravenous injections. All the mice were then injected with [$^{64}$Cu]Cu-NOTA-Anti-mouse CD8 (~50 $\mu$g, ~7.4 Mbq) on day 4 followed by PET imaging on days 5 and 6. The [$^{64}$Cu]Cu-NOTA-anti-mouse CD8 tumor uptake was calculated based on the region of interest (ROI) drawing based on the PET images acquired at 24 h and 48 h timepoint. Bars, n=8 mice per group, mean ± S.E.M. The statically significant differences between experimental groups were performed using analysis of variance (ANOVA) followed by Student's T-test.

**Figure 5. (a)** Schematic of experimental treatment protocol to study the efficacy of click therapy in tumors resistant to T-DXd therapy. Mice xenografted with NCIN87 gastric cancer cells were treated with T-DXd (5 mg $kg^{-1}$), following the tumor volume measurements for a period of ~one month. The mice were then stratified as responders and non-responders based on the tumor volume measurement. Later, the responder mice were kept on the T-DXd therapy whereas the non-responder mice were kept on the click therapy. For click therapy, the first pair of click antibodies *i.e.,* Pan-TCO (5 mg $kg^{-1}$) was injected *via* the tail vein 24 h prior to the injection of T-DXd or T-DXd-Tz (5 mg $kg^{-1}$). Bars, n=4-8 mice per group, mean ± S.E.M. **(b)** Anti-HER2 PET imaging was performed to confirm the responder versus non-responder stratification of mice on day 30. The mice were intravenously injected with [$^{64}$Cu]Cu-NOTA-Trast-Tz (80 $\mu$g, ~10.5-11.84 Mbq) and PET imaging was performed at 24 h timepoint (n=3). **(c)** Western blot showing EGFR

upregulation in non-responder tumors when compared with control. **(d)** The responder mice were kept on the T-DXd therapy (5 mg $kg^{-1}$) whereas the non-responder mice were kept on the click therapy. For click therapy, the first therapy of click antibodies *i.e.,* Pan-TCO (5 mg $kg^{-1}$) was injected *via* the tail vein 24 h prior to the injection of T-DXd or T-DXd-Tz (5 mg $kg^{-1}$). **(e,f)** Efficacy of antibody-ADC click in tumors resistant to trastuzumab therapy. The mice were xenografted with Trastuzumab resistant BT474 cancer cells. The mice were stratified into responder and non-responder therapy mice based on tumor volume measurements. The non-responder mice were kept on the click therapy. For click therapy, the therapy of click pair *i.e.,* Per-TCO (5 mg $kg^{-1}$) was injected *via* the tail vein 24 h prior to the injection of T-DXd or T-DXd-Tz (5 mg $kg^{-1}$).

## REFERENCES


1. Fu, Z., Li, S., Han, S., Shi, C. & Zhang, Y. Antibody drug conjugate: the "biological missile" for targeted cancer therapy. *Signal Transduction and Targeted Therapy* **7**, 93 (2022).
2. Colombo, R. & Rich, J.R. The therapeutic window of antibody drug conjugates: A dogma in need of revision. *Cancer Cell* **40**, 1255-1263 (2022).
3. Drago, J.Z., Modi, S. & Chandarlapaty, S. Unlocking the potential of antibody–drug conjugates for cancer therapy. *Nature Reviews Clinical Oncology* **18**, 327-344 (2021).
4. Tarantino, P. et al. Antibody–drug conjugates: Smart chemotherapy delivery across tumor histologies. *CA: A Cancer Journal for Clinicians* **72**, 165-182 (2022).
5. Kang, J.C. et al. Engineering a HER2-specific antibody–drug conjugate to increase lysosomal delivery and therapeutic efficacy. *Nature Biotechnology* **37**, 523-526 (2019).
6. Beck, A., Goetsch, L., Dumontet, C. & Corvaïa, N. Strategies and challenges for the next generation of antibody–drug conjugates. *Nature Reviews Drug Discovery* **16**, 315-337 (2017).
7. Vasan, N., Baselga, J. & Hyman, D.M. A view on drug resistance in cancer. *Nature* **575**, 299-309 (2019).
8. Li, G. et al. Mechanisms of Acquired Resistance to Trastuzumab Emtansine in Breast Cancer Cells. *Molecular Cancer Therapeutics* **17**, 1441-1453 (2018).
9. Zhao, B., Hemann, M.T. & Lauffenburger, D.A. Intratumor heterogeneity alters most effective drugs in designed combinations. *Proc Natl Acad Sci U S A* **111**, 10773-10778 (2014).

10. Wolchok, J.D. et al. Nivolumab plus Ipilimumab in Advanced Melanoma. *New England Journal of Medicine* **369**, 122-133 (2013).

11. Ott, P.A., Hodi, F.S., Kaufman, H.L., Wigginton, J.M. & Wolchok, J.D. Combination immunotherapy: a road map. *Journal for ImmunoTherapy of Cancer* **5**, 16 (2017).

12. Boutros, C. et al. Safety profiles of anti-CTLA-4 and anti-PD-1 antibodies alone and in combination. *Nature Reviews Clinical Oncology* **13**, 473-486 (2016).

13. Labrijn, A.F., Janmaat, M.L., Reichert, J.M. & Parren, P.W.H.I. Bispecific antibodies: a mechanistic review of the pipeline. *Nature Reviews Drug Discovery* **18**, 585-608 (2019).

14. Filho, O.M. et al. Impact of HER2 Heterogeneity on Treatment Response of Early-Stage HER2-Positive Breast Cancer: Phase II Neoadjuvant Clinical Trial of T-DM1 Combined with Pertuzumab. *Cancer Discovery* **11**, 2474-2487 (2021).

15. Perez, E.A. et al. Trastuzumab Emtansine With or Without Pertuzumab Versus Trastuzumab Plus Taxane for Human Epidermal Growth Factor Receptor 2-Positive, Advanced Breast Cancer: Primary Results From the Phase III MARIANNE Study. *J Clin Oncol* **35**, 141-148 (2017).

16. Fuentes-Antrás, J., Genta, S., Vijenthira, A. & Siu, L.L. Antibody–drug conjugates: in search of partners of choice. *Trends in Cancer* **9**, 339-354 (2023).

17. Hutchings, M. et al. Glofitamab, a Novel, Bivalent CD20-Targeting T-Cell-Engaging Bispecific Antibody, Induces Durable Complete Remissions in Relapsed or Refractory B-Cell Lymphoma: A Phase I Trial. *J Clin Oncol* **39**, 1959-1970 (2021).

18. Zeglis, B.M. & Lewis, J.S. Click Here for Better Chemistry. *N Engl J Med* **387**, 2291-2293 (2022).

19. Peplow, M. 'Clicked' drugs: researchers prove the remarkable chemistry in humans. *Nature Biotechnology* **41**, 883-885 (2023).

20. Kolb, H.C., Finn, M.G. & Sharpless, K.B. Click Chemistry: Diverse Chemical Function from a Few Good Reactions. *Angewandte Chemie International Edition* **40**, 2004-2021 (2001).

21. Tornøe, C.W. & Meldal, M. Peptides 2001 Proc. Am. Pept. Symp. (2001).

22. Tornøe, C.W., Christensen, C. & Meldal, M. Peptidotriazoles on Solid Phase: [1,2,3]-Triazoles by Regiospecific Copper(I)-Catalyzed 1,3-Dipolar Cycloadditions of Terminal Alkynes to Azides. *The Journal of Organic Chemistry* **67**, 3057-3064 (2002).

23. Saxon, E. & Bertozzi, C.R. Cell surface engineering by a modified Staudinger reaction. *Science* **287**, 2007-2010 (2000).

24. Sangeetha, S. et al. SQ3370, the first clinical click chemistry-activated cancer therapeutic, shows safety in humans and translatability across species. *bioRxiv*, 2023.2003.2028.534654 (2023).

25. Bai, X. et al. Structure and dynamics of the EGFR/HER2 heterodimer. *Cell Discovery* **9**, 18 (2023).

26. Krause, D.S. & Van Etten, R.A. Tyrosine Kinases as Targets for Cancer Therapy. *New England Journal of Medicine* **353**, 172-187 (2005).

27. Cheng, H. et al. EGFR expression is associated with decreased benefit from trastuzumab in the NCCTG N9831 (Alliance) trial. *Br J Cancer* **111**, 1065-1071 (2014).

28. Friedman, L.M. et al. Synergistic down-regulation of receptor tyrosine kinases by combinations of mAbs: Implications for cancer immunotherapy. *Proceedings of the National Academy of Sciences* **102**, 1915-1920 (2005).

29. von Minckwitz, G. et al. Trastuzumab Emtansine for Residual Invasive HER2-Positive Breast Cancer. *New England Journal of Medicine* **380**, 617-628 (2018).

30. Mestel, R. Cancer: Imaging with antibodies. *Nature* **543**, 743-746 (2017).

31. Sharma, S.K. et al. Influence of Fc Modifications and IgG Subclass on Biodistribution of Humanized Antibodies Targeting L1CAM. *J Nucl Med* **63**, 629-636 (2022).

32. Bouleau, A. et al. Optimizing Immuno-PET Imaging of Tumor PD-L1 Expression: Pharmacokinetic, Biodistribution, and Dosimetric Comparisons of (89)Zr-Labeled Anti-PD-L1 Antibody Formats. *J Nucl Med* **63**, 1259-1265 (2022).

33. Nakamura, Y. et al. Circulating tumor DNA-guided treatment with pertuzumab plus trastuzumab for HER2-amplified metastatic colorectal cancer: a phase 2 trial. *Nature Medicine* **27**, 1899-1903 (2021).

34. Franklin, M.C. et al. Insights into ErbB signaling from the structure of the ErbB2-pertuzumab complex. *Cancer Cell* **5**, 317-328 (2004).

35. Takegawa, N. et al. DS-8201a, a new HER2-targeting antibody–drug conjugate incorporating a novel DNA topoisomerase I inhibitor, overcomes HER2-positive gastric cancer T-DM1 resistance. *International Journal of Cancer* **141**, 1682-1689 (2017).

36. Rao, Y. et al. Statins enhance the efficacy of HER2-targeting radioligand therapy in drug-resistant gastric cancers. *Proc Natl Acad Sci U S A* **120**, e2220413120 (2023).

37. Cortés, J. et al. Trastuzumab Deruxtecan versus Trastuzumab Emtansine for Breast Cancer. *New England Journal of Medicine* **386**, 1143-1154 (2022).

38. Mosele, F. et al. Trastuzumab deruxtecan in metastatic breast cancer with variable HER2 expression: the phase 2 DAISY trial. *Nature Medicine* **29**, 2110-2120 (2023).

39. von Minckwitz, G. et al. Adjuvant Pertuzumab and Trastuzumab in Early HER2-Positive Breast Cancer. *New England Journal of Medicine* **377**, 122-131 (2017).

40. Pereira, P.M.R. et al. Caveolin-1 mediates cellular distribution of HER2 and affects trastuzumab binding and therapeutic efficacy. *Nature Communications* **9**, 5137 (2018).

41. Pereira, P.M.R. et al. Caveolin-1 temporal modulation enhances antibody drug efficacy in heterogeneous gastric cancer. *Nature Communications* **13**, 2526 (2022).

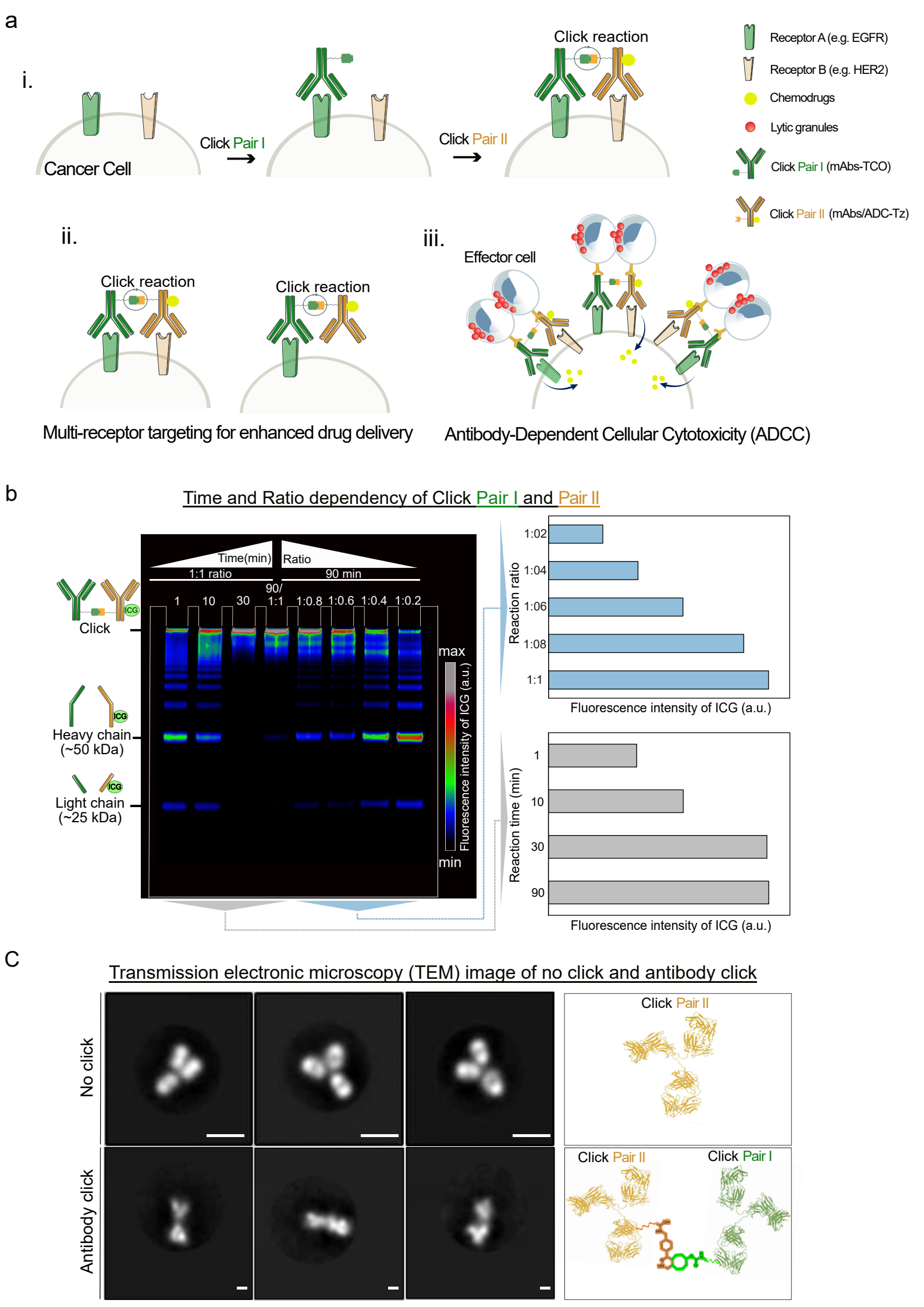
a
i.
Cancer Cell
Click Pair I
Click reaction
Click Pair II
Receptor A (e.g. EGFR)
Receptor B (e.g. HER2)
Chemodrugs
Lytic granules
Click Pair I (mAbs-TCO)
Click Pair II (mAbs/ADC-Tz)
ii.
Click reaction
Click reaction
Multi-receptor targeting for enhanced drug delivery
iii.
Effector cell
Antibody-Dependent Cellular Cytotoxicity (ADCC)
b
Time and Ratio dependency of Click Pair I and Pair II
Time(min)
Ratio
1:1 ratio
90 min
1
10
30
90/
1:1
1:0.8
1:0.6
1:0.4
1:0.2
Click
Heavy chain
(~50 kDa)
Light chain
(~25 kDa)
ICG
max
min
Fluorescence intensity of ICG (a.u.)
Reaction ratio
1:02
1:04
1:06
1:08
1:1
Fluorescence intensity of ICG (a.u.)
Reaction time (min)
1
10
30
90
Fluorescence intensity of ICG (a.u.)
C
Transmission electronic microscopy (TEM) image of no click and antibody click
No click
Antibody click
Click Pair II
Click Pair II
Click Pair I

a

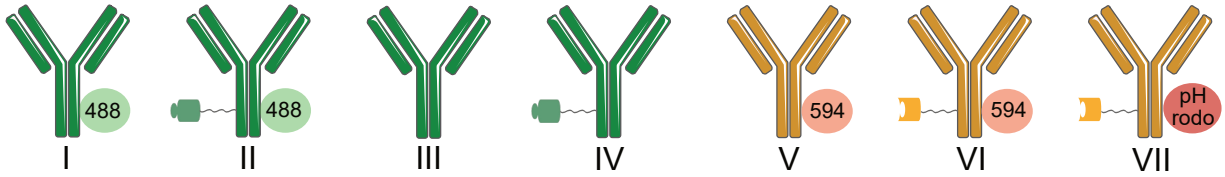


| | I | II | III | IV | V | VI | VII |
|---|---|---|---|---|---|---|---|
| HER2 targeting | - | - | - | - | + | + | + |
| EGFR targeting | + | + | + | + | - | - | - |
| TCO | - | + | - | + | - | - | - |
| Tz | - | - | - | - | - | + | + |
| Alexa-488 | + | + | - | - | - | - | - |
| Alexa-594 | - | - | - | - | + | + | - |
| pHrodo | - | - | - | - | - | - | + |

b

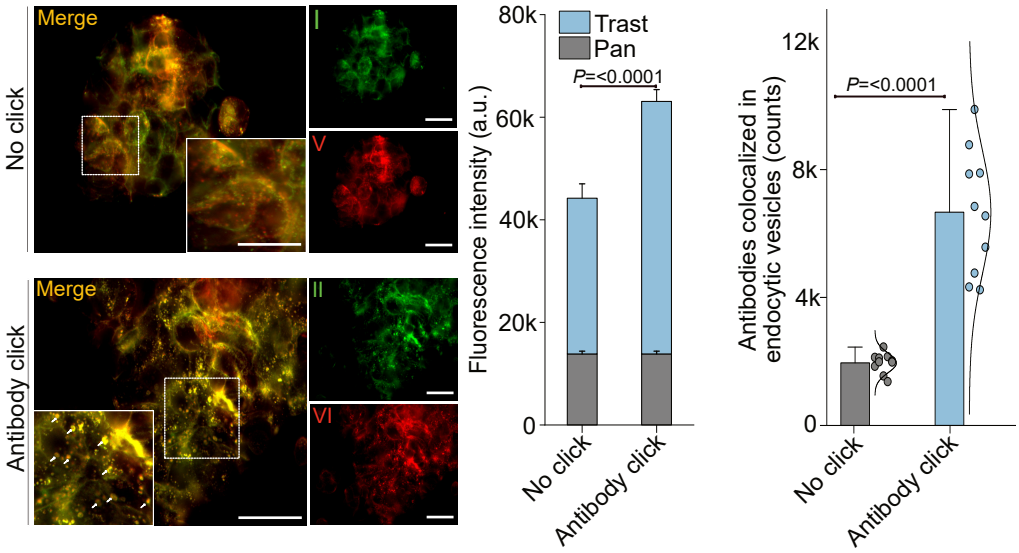


c

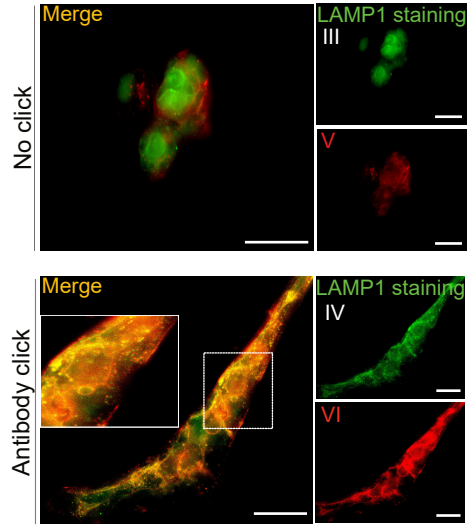


d

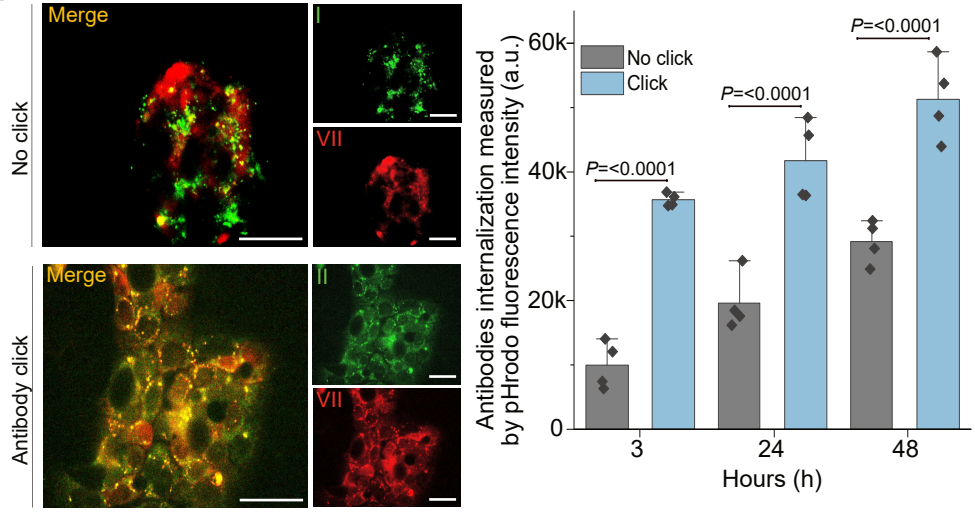


e

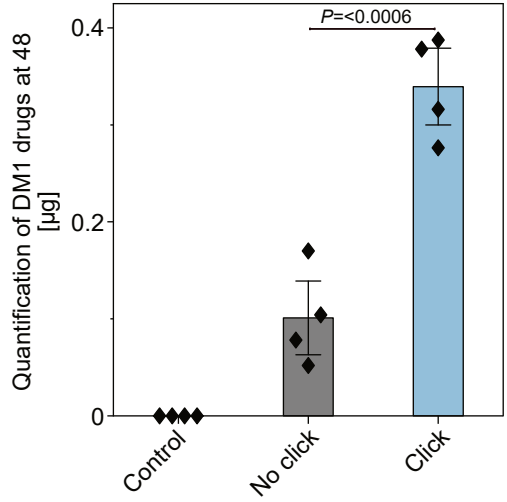

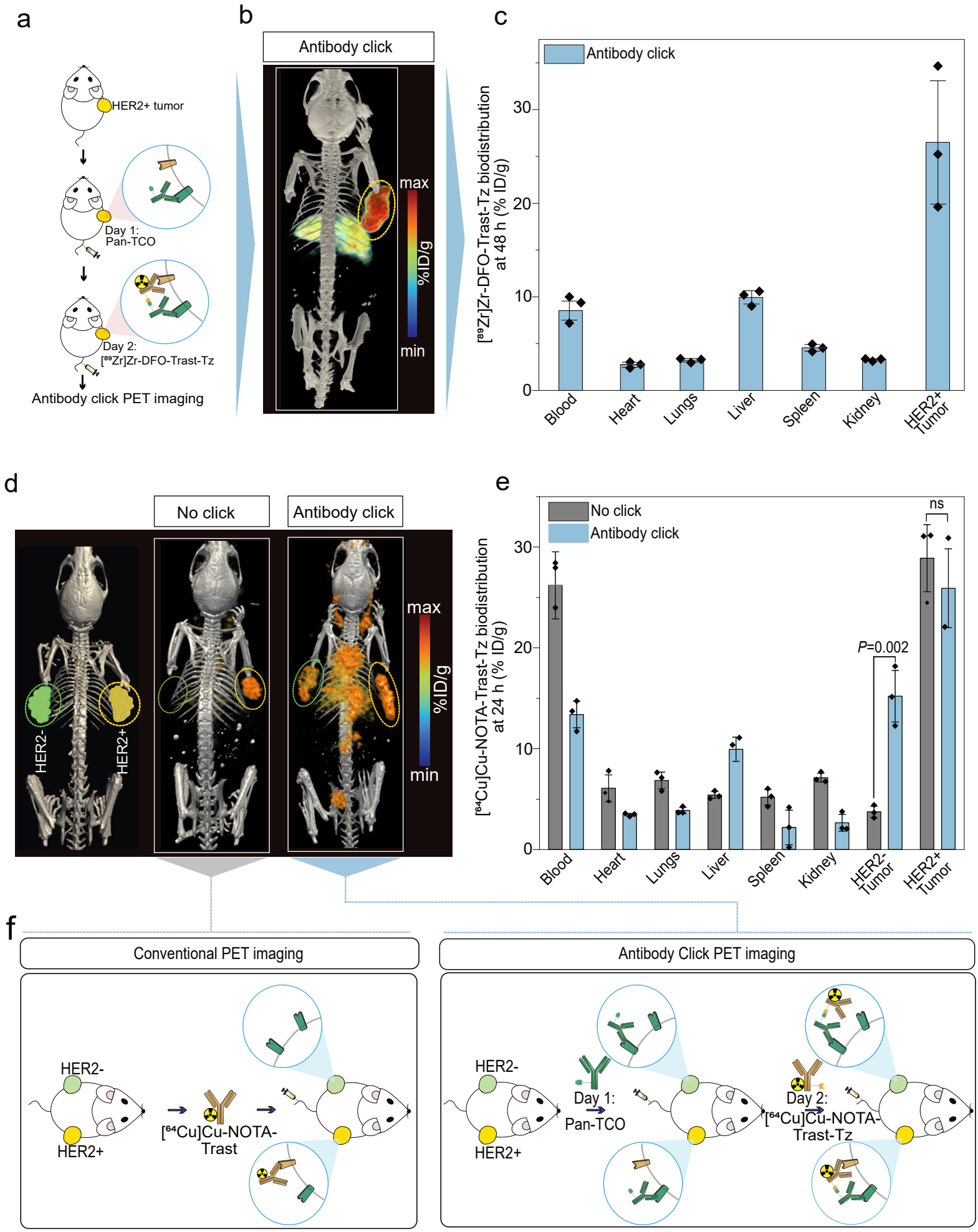
a
HER2+ tumor
Day 1:
Pan-TCO
Day 2:
[89Zr]Zr-DFO-Trast-Tz
Antibody click PET imaging
b
Antibody click
max
%ID/g
min
c
Antibody click
[89Zr]Zr-DFO-Trast-Tz biodistribution at 48 h (% ID/g)
0
10
20
30
Blood
Heart
Lungs
Liver
Spleen
Kidney
HER2+ Tumor
d
No click
Antibody click
HER2-
HER2+
max
%ID/g
min
e
No click
Antibody click
ns
P=0.002
[64Cu]Cu-NOTA-Trast-Tz biodistribution at 24 h (% ID/g)
0
10
20
30
Blood
Heart
Lungs
Liver
Spleen
Kidney
HER2- Tumor
HER2+ Tumor
f
Conventional PET imaging
HER2-
HER2+
[64Cu]Cu-NOTA-Trast
Antibody Click PET imaging
HER2-
HER2+
Day 1:
Pan-TCO
Day 2:
[64Cu]Cu-NOTA-Trast-Tz

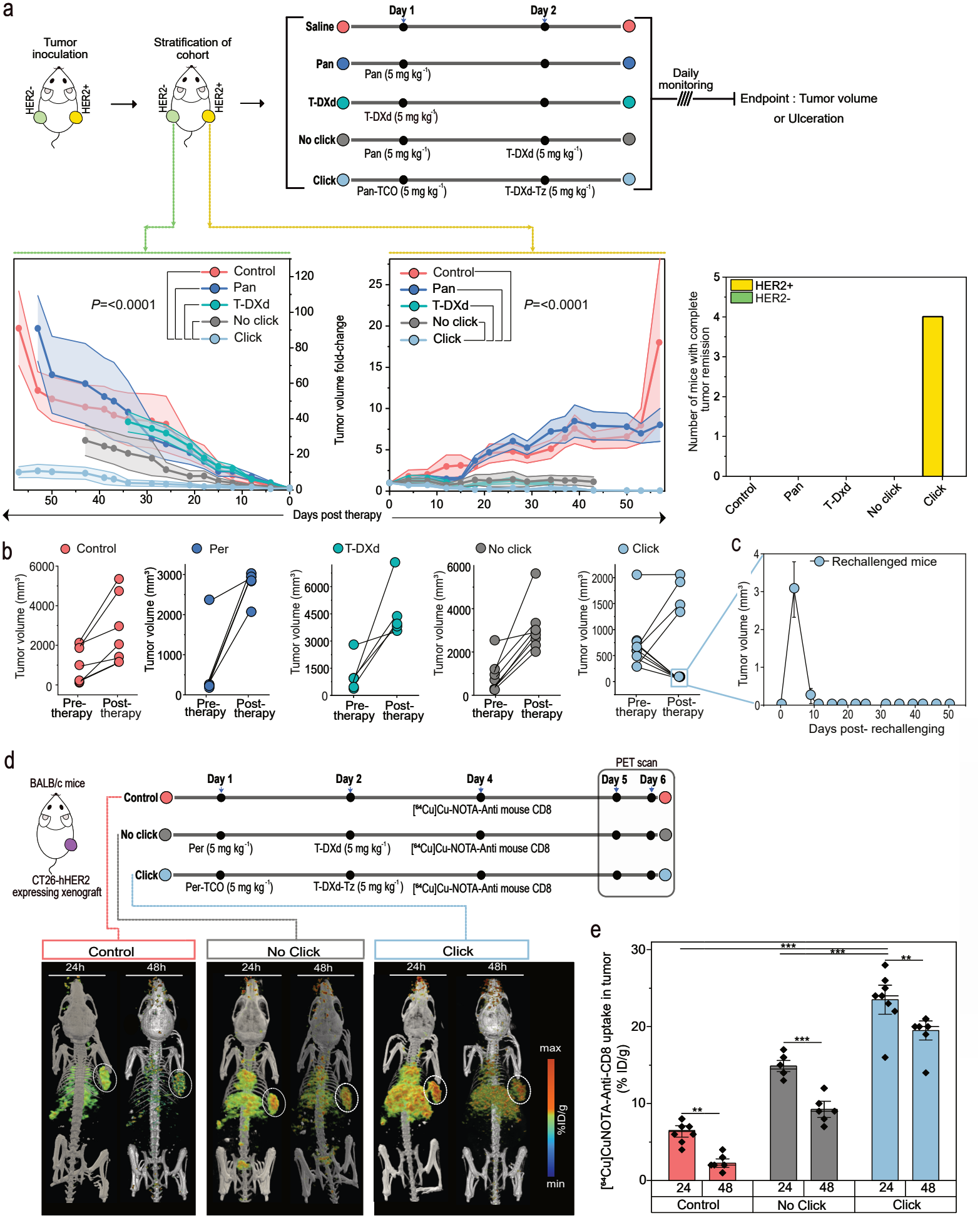
a
Tumor inoculation
HER2-
HER2+
Stratification of cohort
Day 1
Day 2
Saline
Pan
Pan (5 mg kg-1)
T-DXd
T-DXd (5 mg kg-1)
No click
Pan (5 mg kg-1)
T-DXd (5 mg kg-1)
Click
Pan-TCO (5 mg kg-1)
T-DXd-Tz (5 mg kg-1)
Daily monitoring
Endpoint : Tumor volume or Ulceration
Control
Pan
T-DXd
No click
Click
P=<0.0001
Tumor volume fold-change
Days post therapy
HER2+
HER2-
Number of mice with complete tumor remission
b
Per
Tumor volume (mm3)
Pre-therapy
Post-therapy
c
Rechallenged mice
Days post- rechallenging
d
BALB/c mice
CT26-hHER2 expressing xenograft
PET scan
Day 4
Day 5
Day 6
[64Cu]Cu-NOTA-Anti mouse CD8
Per (5 mg kg-1)
Per-TCO (5 mg kg-1)
T-DXd-Tz (5 mg kg-1)
24h
48h
max
min
%ID/g
e
[64Cu]CuNOTA-Anti-CD8 uptake in tumor (% ID/g)
No Click

a

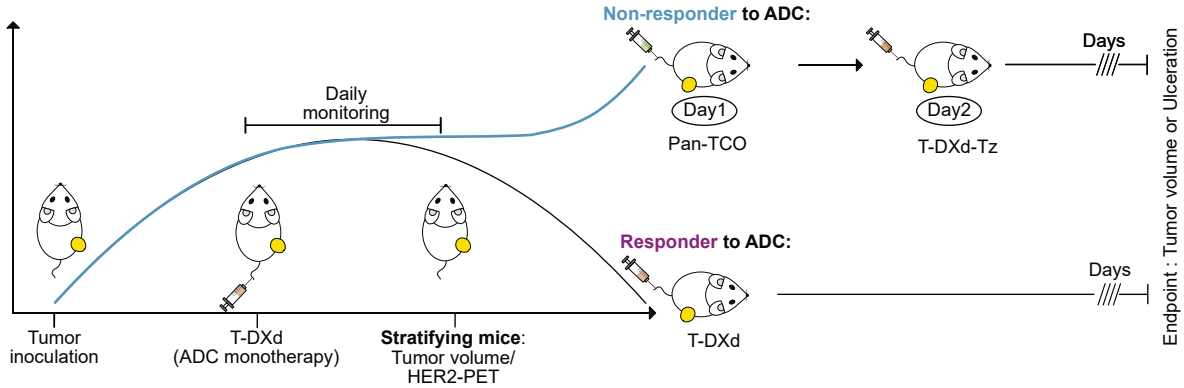
Non-responder to ADC:
Day1
Pan-TCO
Day2
T-DXd-Tz
Days
Daily monitoring
Responder to ADC:
T-DXd
Days
Endpoint : Tumor volume or Ulceration
Tumor inoculation
T-DXd (ADC monotherapy)
Stratifying mice: Tumor volume/ HER2-PET

b

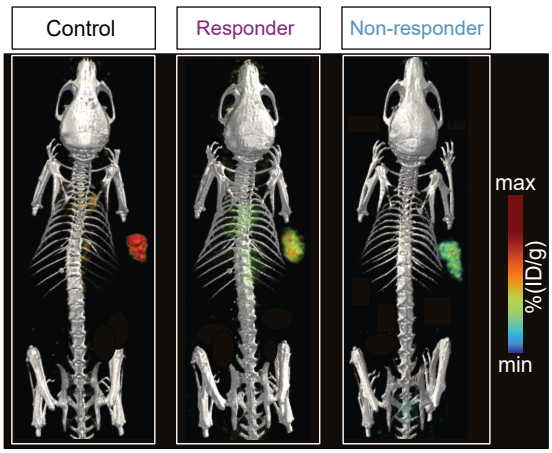
Control
Responder
Non-responder
max
%(ID/g)
min

c

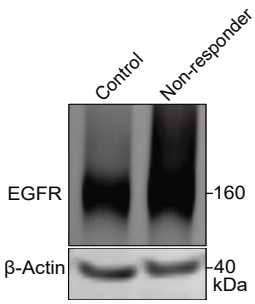
Control
Non-responder
EGFR
160
β-Actin
40
kDa

d

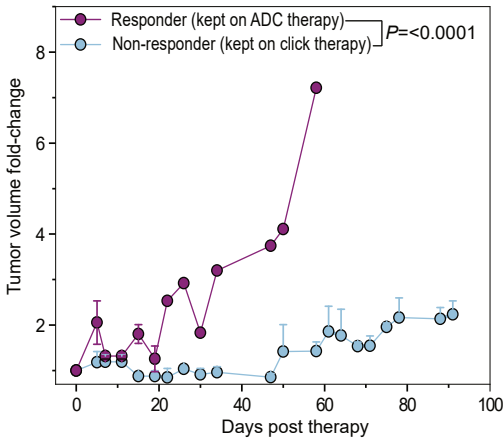
Responder (kept on ADC therapy)
Non-responder (kept on click therapy)
P=<0.0001
Tumor volume fold-change
Days post therapy

e

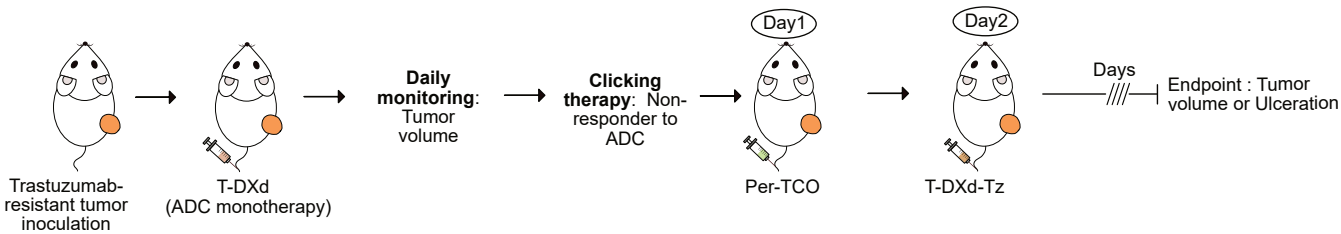
Trastuzumab-resistant tumor inoculation
T-DXd (ADC monotherapy)
Daily monitoring: Tumor volume
Clicking therapy: Non-responder to ADC
Day1
Per-TCO
Day2
T-DXd-Tz
Days
Endpoint : Tumor volume or Ulceration

d

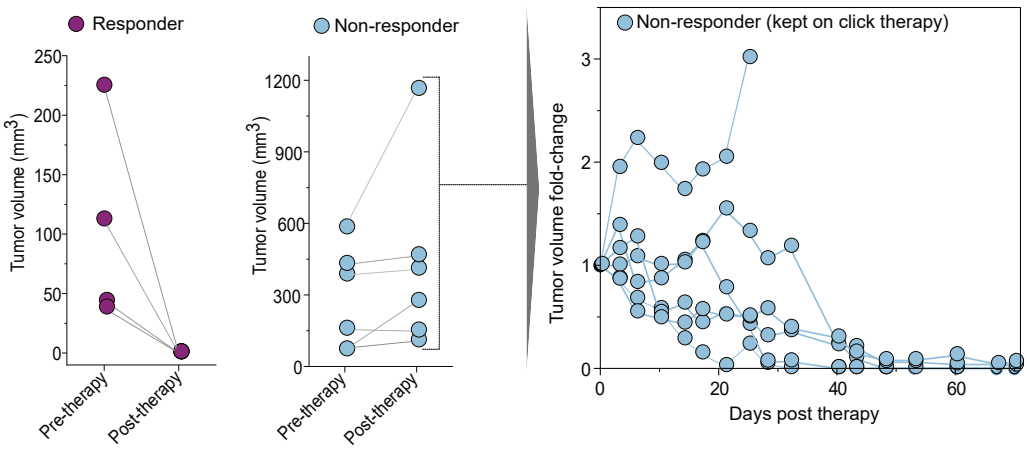
Responder
Non-responder
Tumor volume (mm3)
Pre-therapy
Post-therapy
Non-responder (kept on click therapy)
Tumor volume fold-change
Days post therapy